Influence of tropical easterly jet on upper tropical cirrus: An observational study from CALIPSO, Aura-MLS, and NCEP/NCAR data

Subrata Kumar Das,[1,2] Chih-Wei Chiang,[1,3] and Jan-Bai Nee[1]

Received 9 March 2011; revised 9 March 2011; accepted 22 March 2011; published 21 June 2011.

[1] The role of the redistribution of tropical upper tropospheric humidity in the formation of tropical cirrus is studied using three years (June 2006 to December 2008) of observations with the Cloud-Aerosol Lidar with Orthogonal Polarization (CALIOP) instrument onboard the Cloud-Aerosol Lidar and Infrared Pathfinder Satellite Observation (CALIPSO) as well as the Microwave Limb Sounder (MLS) onboard the Aura satellite. The National Centers for Environmental Prediction and Atmospheric Research reanalysis data are also used. Results show that the redistribution of upper tropospheric humidity from a highly convective zone to the Indian peninsular region leads to the formation of the tropical cirrus. Advection of upper layer humidity is caused by the tropical easterly jet (TEJ) associated with the Asian summer monsoon (ASM). Thus the present analysis brings out, for the first time, the role of the TEJ in the redistribution of upper tropospheric humidity and consequently in the formation of tropical cirrus. As little observational evidence exists in support of the generative mechanisms of the cirrus, the present results can be useful in quantifying the formation process of these clouds, which have implications for Earth's radiation budget and improving global climate models.

Citation: Das, S. K., C.-W. Chiang, and J.-B. Nee (2011), Influence of tropical easterly jet on upper tropical cirrus: An observational study from CALIPSO, Aura-MLS, and NCEP/NCAR data, *J. Geophys. Res.*, *116*, D12204, doi:10.1029/2011JD015923.

1. Introduction

[2] Upper tropospheric water vapor has important implications in the chemical and physical properties of the tropical tropopause layer, terrestrial radiation budget, and stratospheric chemistry. The processes that govern the entry of moist air into the tropical upper troposphere and lower stratosphere (UTLS) are a combination of (1) rapid vertical motion, i.e., rapid overshooting convection, and (2) slow diabatic ascent, i.e., a freeze-drying mechanism due to low temperature, in the vicinity of the tropical tropopause [*Gettelman et al.*, 2002, and references therein]. The global distribution of upper tropospheric water vapor is not fully understood due to its low density and uncertainties in its concentration in the UTLS region [*Park et al.*, 2007]. The Microwave Limb Sounder (MLS) onboard the Aura satellite provides a better opportunity to study the global upper tropospheric water vapor [*Waters et al.*, 2006]. Several studies have examined the global distribution of upper tropospheric water vapor by using the measurements from the Aura-MLS, especially over the tropics [*Park et al.*, 2007; *James et al.*, 2008]. However, there are still open scientific problems in the redistribution and variation of water vapor and their controlling mechanisms in the upper troposphere, especially in the region of the South Asian summer monsoon (ASM hereafter). The ASM is an anticyclone system in the UTLS region during Northern Hemisphere (NH) summer. The anticyclone encompasses an easterly jet in the tropics and a westerly jet in the midlatitudes. Recent studies have found that the anticyclone circulation is important in the distribution of various trace species [*Park et al.*, 2007].

[3] There are two important aspects of the upper tropospheric water vapor: (1) its role in the formation of tropical cirrus and (2) the dehydration mechanism in the upper troposphere [*Platt*, 1973; *Liou*, 1986; *Twomey*, 1991]. These factors are important for understanding the formation of cirrus clouds, which cover almost 20% of the Earth's surface [*Liou*, 1986; *Heymsfield and McFarquhar*, 2002], out of which 50% is over the tropical regions. Cirrus clouds are believed to have a profound effect upon the planetary energy budget due to their radiative properties [*Wang et al.*, 1996]. Critical parameters in understanding the radiative effects of cirrus clouds are their geometrical and optical thickness along with occurrence height and other microphysical properties such as the shape and size of the ice crystals.

[1]Department of Physics, National Central University, Chung-Li, Taiwan.
[2]Now at PM&A Division, Indian Institute of Tropical Meteorology, Pune, India.
[3]Research Center for Environmental Changes, Academia Sinica, Taipei, Taiwan.

0148-0227/11/2011JD015923

However, the processes involved in the formation of cirrus clouds are not well understood, and thus they are poorly represented in global climate models [*Penner et al.*, 1999].

[4] According to current theory, there are two primary mechanisms important for the formation of tropical cirrus: (1) convective transport of water vapor to the upper part of the troposphere by cumulonimbus clouds (i.e., anvil cirrus), and (2) in situ formation of ice crystals by slow, synoptic scale uplift of a humid layer (i.e., in situ cirrus) [*Jensen et al.*, 1996]. The maximum amount of water vapor in the UTLS during the NH summer is observed over the ASM regions [*Park et al.*, 2007], which coincides well with the frequent observations of cirrus clouds as will be shown in this paper and also discussed by *Sassen et al.* [2008].

[5] The occurrence of a tropical easterly jet (TEJ) in the NH summer is one of the prominent features associated with the ASM [*Sathiyamoorthy et al.*, 2007]. The TEJ is usually observed in the longitudes 20°E–140°E and latitudes 5°S–20°N. The TEJ is generally maintained by the thermal gradient present in the upper troposphere between the heated Asian landmasses of the Tibetan high plateau and relatively cooler Indian Ocean during the ASM season [*Koteswaram*, 1958]. The TEJ formed over the South Asia–Pacific region lies at heights of 200–100 hPa pressure levels with wind speeds reaching up to 40 m s^{-1} [*Hastenrath*, 1991]. It can redistribute the water vapor including liquid/ice particles brought up by deep convection and can form high-altitude clouds [*Ahrens*, 2003; *Sathiyamoorthy et al.*, 2004]. It should be noted that only a few studies have been done previously to examine the relationship between the TEJ and cirrus clouds. This lack can be attributed to the complex physical properties of cirrus clouds and the TEJ, which makes their measurements difficult and thus limited. In addition, synoptic scale disturbances such as jet streams, frontal and low pressure systems [*De Mott*, 2002; *Khvorostyanov and Sassen*, 2002], deep convection [*Mace et al.*, 2006], orographic/terrain-induced cirrus [*Wylie*, 2002], and exhaust from jet traffic [*Schumann*, 2002] also contribute to the formation of the tropical cirrus. However, over the middle and high latitudes, the bulk of cirrus is formed by baroclinic fronts [*Liou*, 1986]. It is evident from the above studies that the formation, maintenance, and dissipation of cirrus clouds are directly associated with the large-scale synoptic features or disturbances and are also partly related to the cumulonimbus outflows. While the mechanisms are qualitatively understood, the quantitative basis for their formation and dissipation has not yet been addressed.

[6] Several studies have contributed greatly to our knowledge of the fundamental properties of cirrus clouds by using different techniques [e.g., *Francis et al.*, 1999; *Sassen and Mace*, 2002, and references therein]. However, each approach has its own pros and cons. Ground measurements have a limited global coverage and are also adversely affected by the presence of low-level clouds. On the other hand, aircraft measurements that can provide the horizontal structure of the cloud are limited to the cruising altitudes. *Sassen et al.* [2008, and references therein] reported that the studies on the vertical structure of the cirrus clouds on a global scale were traditionally limited due to the irregular space-time sampling from the ground-based as well as from the satellite observations. With the advent of the Cloud-Aerosol Lidar with Orthogonal Polarization (CALIOP) instrument onboard the Cloud-Aerosol Lidar and Infrared Pathfinder satellite Observation (CALIPSO), which is a spaceborne lidar, we can now study the vertical and global distributions of cirrus clouds. For example, by using CALIPSO observations, *Lamquin et al.* [2008] reported that the geometrical thickness of cirrus has a greater influence than the optical depth on the relative humidity of ambient air. *Sassen et al.* [2008] studied the global and seasonal distribution of cirrus clouds and found an average occurrence frequency of about 16.7%, based on CALIPSO observations. Several other studies have also reported the global characteristics of cirrus cloud using CALIPSO data [*Nazaryan et al.*, 2008; *Sassen et al.*, 2009]. However, these studies have not dealt with the generative mechanisms of cirrus clouds and the role of the TEJ in their distribution/formation process. These aspects form the basis for the present study.

[7] Realizing the importance of the global distribution of upper humidity in the formation of the tropical cirrus, we attempt for the first time to show the role of the TEJ in this context. In this study, we analyze the monthly distribution of global upper tropospheric humidity and tropical cirrus and their association with the TEJ. We also use the wind, temperature, and outgoing longwave radiation (OLR) data from the National Centers for Environmental Prediction/National Center for Atmospheric Research (NCEP/NCAR) reanalysis to investigate the characteristics of the TEJ, temperature anomalies, and the intensity of convection, respectively. In the following section, a brief description of the instruments and data used is given. Section 3 presents the results and discussion. Finally, summary and concluding remarks are given in section 4.

2. Instrumentation and Data Analysis

[8] The CALIPSO satellite was launched on 28 April 2006 orbiting the Earth as a cluster with other NASA spacecrafts in the A-Train platform. It is a nadir-viewing, sun-synchronous satellite, designed to study the impact of clouds and aerosols on the radiation budget and the climate of the Earth [*Winker et al.*, 2003]. CALIOP is a spaceborne lidar system for a long-duration mission designed to detect the clouds and aerosols. Traditionally, the lidar technique uses polarization measurements to detect and differentiate the vertical distribution of water clouds, ice clouds, and aerosol masses [*Sassen*, 1991; *Winker et al.*, 2003]. CALIOP also works on the above principle, taking measurements at wavelengths of 532 nm and 1064 nm with a vertical resolution of 60 m between the height range of 8.2–20.2 km, a region where high-altitude clouds are situated. It has a horizontal resolution of 333 m [*Winker et al.*, 2003]. Details of CALIOP measurements and technical features can be found elsewhere (http://eosweb.larc.nasa.gov/PRODOCS/calipso/table_calipso.html).

[9] The CALIPSO data have been validated by several earlier studies [*Kim et al.*, 2008; *Tao et al.*, 2008]. The present study uses CALIPSO level 2, 5 km (horizontal resolution) cloud layer data product. This product provides information about the geometric thickness and the top and base altitudes of clouds. The confidence level for the identification of the cloud layer is based on the cloud-aerosol discrimination (CAD) score, where the positive (negative) value signifies clouds (aerosols). We have considered only those cloud layers for which the "CAD_Score" parameter is

between 80 and 100 to ensure the high level of confidence in the detection of clouds. For each cloud layer retrieved, an opacity flag parameter is also considered. Only those layers having an "Opacity_Flag" parameter equal to 0 are used in the present study to ensure the cloud layer is transparent. Furthermore, the detection of the lower cloud layer in a multilayer case is more complex, since there can be attenuation of CALIOP signals by the cloud layers above it. However, we have considered only the top layer clouds, and thus the above condition will not affect our results. Detailed descriptions of the detection algorithm of the cloud layer can be found at the Website http://eosweb.larc.nasa.gov/PRODOCS/calipso/Quality_Summaries/CALIOP_L2LayerProducts_2.01.html and references therein.

[10] The data at 532 nm are used in the present study because of their better capability in detecting thin cirrus. Moreover, only nighttime data are considered due to the better signal-to-noise ratio, which makes the detection of thin clouds more reliable [*Winker et al.*, 2003]. Furthermore, in order to avoid the ambiguity of cirrus clouds in polar and Arctic regions, we restricted our analysis to 55°S–55°N latitudes. We define a cirrus cloud using a cloud base height threshold of 8 km in the tropics (25°S–25°N), and 6 km in the midlatitudes (25°S–55°S and 25°N–55°N) [*Dowling and Radke*, 1990]. The calculation of cirrus cloud occurrence frequency is made by using a domain of 10° latitude × 20° longitude.

[11] The MLS instrument onboard the Aura satellite was launched on 15 July 2004 as a part of the A-Train platform. The MLS measures thermal emissions in the millimeter and submillimeter wavelengths by scanning the Earth's atmospheric limb to determine profiles of humidity, temperature, and trace atmospheric species such as O_3, N_2O, HCL, HNO_3, and CO among others. The instrument uses seven radiometers to cover five broad spectral regions between 118 GHz and 2.5 THz. More details about the instrument, algorithms, and science products can be found in the work of *Waters et al.* [2006] and in the MLS webpage (http://mls.jpl.nasa.gov).

[12] In this analysis, we use version 2, level 2 (V2.2) data products of relative humidity at pressure levels of 215, 146, 100, and 82 hPa (corresponding to the altitudes of 12–12.5, 14–14.5, 16–16.5, and 17.5–18 km, respectively). The processing of the MLS data has been described by *Livesey et al.* [2007]. Note that the measurements of the MLS satellite trail the CALIPSO satellite by ~7 min, which is equivalent to a spatial difference of about 1.8° west with respect to the CALIPSO satellite. Since the observations are averaged over a grid of 10° × 20° latitude-longitude for the analysis, some of the data points of both instruments did not fall in the same box. However, in the present study, the large-scale monthly averages are performed, so that spatial lags will have negligible impact on the results. After May 2008, the MLS satellite was relocated much closer to CALIPSO [*Wu et al.*, 2008; *Savtchenko et al.*, 2008] and both measurements can be considered as simultaneous and colocated. Despite this relocation of the satellite track, there are no noticeable differences in the results reported here. As discussed in section 1, the NCEP/NCAR reanalysis data are used to derive the following parameters: (1) zonal and meridonal wind pattern to study the TEJ [*Kalnay et al.*, 1996], (2) OLR as a proxy for the intensity of convection [*Liebmann and Smith*, 1996], and (3) temperature anomaly [*Basist and Chelliah*, 1997]. These data are available as the daily/monthly means, at a grid resolution of 2.5° latitude × 2.5° longitude.

3. Results and Discussion

[13] In an attempt to understand the origin of the tropical cirrus associated with the ASM, we have analyzed the occurrence of cirrus clouds from the CALIPSO data and the wind characteristics from the NCEP/NCAR reanalysis during the period of July 2006 to December 2008. According to the India Meteorological Department (IMD), which follows the World Meteorological Organization (WMO) classification, June to September is considered the ASM period and is referred as the Indian summer monsoon (ISM), especially over the Indian region. Since we are interested in the role of the TEJ in the formation and/or transport of the tropical cirrus, we restrict our analysis to the period ranging from June to September of 2006–2008.

[14] Figure 1 shows contour maps of the monthly frequency distribution of cirrus clouds derived from CALIPSO observations for the period June to September 2006–2008. The first panel (June 2006) is left blank as there are limited observations of CALIPSO for that month. The thick, dark closed contours indicate the locations of OLR <220 W m^{-2} for the corresponding month. The threshold of OLR <220 W m^{-2} is considered the proxy of convection, because this condition is expected to have more deep convective clouds and have more moisture content [e.g., *Wild and Roeckner*, 2006; *Ricaud et al.*, 2007]. The cirrus cloud frequency is calculated by taking the ratio of the cirrus observed to the total number of observations made within each grid of 10° latitude × 20° longitude for each month. These contour maps clearly depict that the maximum occurrence of cirrus clouds is over the Indian tropical region (15°S–25°N and 30°E–170°E), i.e., the ASM region, and over some parts of central west Africa. However, comparatively less cirrus clouds are observed over the northern part of South America (not shown). These results are consistent with earlier reports [e.g., *Wylie et al.*, 1994; *Wang et al.*, 1996], suggesting that the general characteristics of the cirrus distributions are the persistent features of the atmosphere. *Yang et al.* [2010] investigated the optical depth of the top layer of cirrus clouds by using one year of CALIPSO data. They found that a large fraction of thin cirrus (optical depth <0.3) is distributed over the Indian tropical regions during the summer (June to August), which are the same areas considered in the present study. The optically thin cirrus cloud plays a crucial role in the Earth's radiation budget and in determining the mass exchange between the troposphere and stratosphere [*Hartmann et al.*, 2001; *Corti et al.*, 2005].

[15] From Figure 1, it can be seen that over the regions of the Indian peninsula and the West Bay of Bengal, cirrus clouds occur more frequently in June–July than August–September. However, over the Bay of Bengal, the occurrence of cirrus remains uniform from June to September. One striking feature to be noted is that in the initial phase of the ASM in June, the occurrence of cirrus is elongated along the longitude, but this cirrus is confined to the Indian peninsular region by the end of the ASM in September. *Nazaryan et al.* [2008] and *Sassen et al.* [2008] also analyzed CALIPSO data

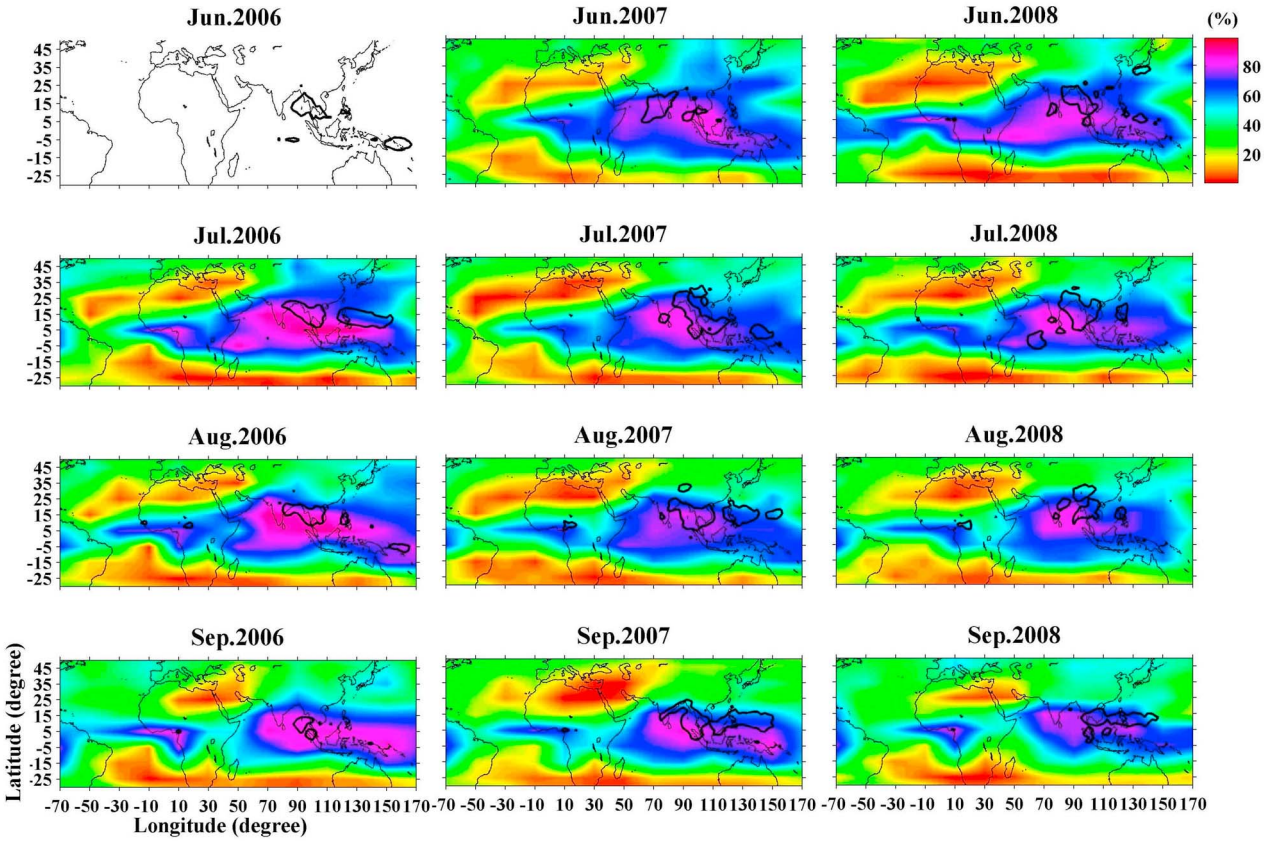

Figure 1. Contour map of the monthly distribution of cirrus occurrence derived from the CALIPSO during June to September in the years 2006–2008. The closed thick contours indicate the outgoing longwave radiation (OLR) <220 W m^{-2}. The OLR data is taken from the NCEP/NCAR reanalysis. The blank areas denote no data.

and showed that the occurrence of cirrus peaked over the Indian peninsular region. Figure 1 also reveals that OLR, which is a proxy for convective activity, is low (<220 W m^{-2}) and is confined to a smaller area as compared with the extended occurrence of cirrus. *Clark* [2005] reported that the formation of cirrus clouds is favored over deep convective regions (low OLR). *Sherwood and Dessler* [2003] pointed out that convection can be one of the processes to supply water vapor to form cirrus in the vicinity of the tropical tropopause given that there is negligible horizontal transport of water vapor from the extratropical areas. However, from Figure 1 one can find that the cirrus clouds occur in regions of high OLR (>220 W m^{-2}), which could be attributed to the slow advection takes place over these areas, suggesting that other factors besides convection also influence the formation and distribution of cirrus. The maximum occurrence of cirrus over the Indian and the Southeast Asian regions during the ASM may be due to the large amount of moisture present in the atmosphere associated with convection and advection, which will be discussed later.

[16] Figures 2a, 2b, 2c, and 2d show contour maps of monthly mean relative humidity with respect to ice (RHi) at different pressure levels (215, 146, 100, and 82 hPa) during June to September, respectively, for the years 2006–2008. These contour maps clearly indicate that the maximum amount of water vapor is available over the tropical areas around 15°S–25°N and 30°E–170°E, i.e., around the ASM region at the 215 hPa pressure level. However, in the upper height levels, water vapor is confined to nearly 15°N–25°N and 30°E–110°E. It is possible that the overshooting convection plays a major role in the transport of water vapor into the upper troposphere. As mentioned earlier, since the intensity of convection (OLR <220 W m^{-2}) is confined to smaller areas, it is believed that convection is not the only process that governs the distribution of water vapor in the upper troposphere. The process which controls the water vapor near the tropopause (100 hPa) is very complex and yet to be understood [*Park et al.*, 2007]. It is also to be noted that at the 925 hPa pressure level, the maximum amount of humidity is confined in the vicinity of low OLR, i.e., over the North Bay of Bengal, as revealed by the NCEP/NCAR reanalysis (not shown).

[17] To gain further insight, we have analyzed monthly mean vertical velocity obtained from the NCEP/NCAR reanalysis for 2006–2008 at 250 hPa and 100 hPa pressure levels, which are shown in Figures 3a and 3b, respectively. The color bars with positive (negative) values signify the upward (downward) motion. A strong updraft of the order >2 cm s^{-1} is observed over the ASM region. This shows that due to convection, the moisture rises from the lower to the

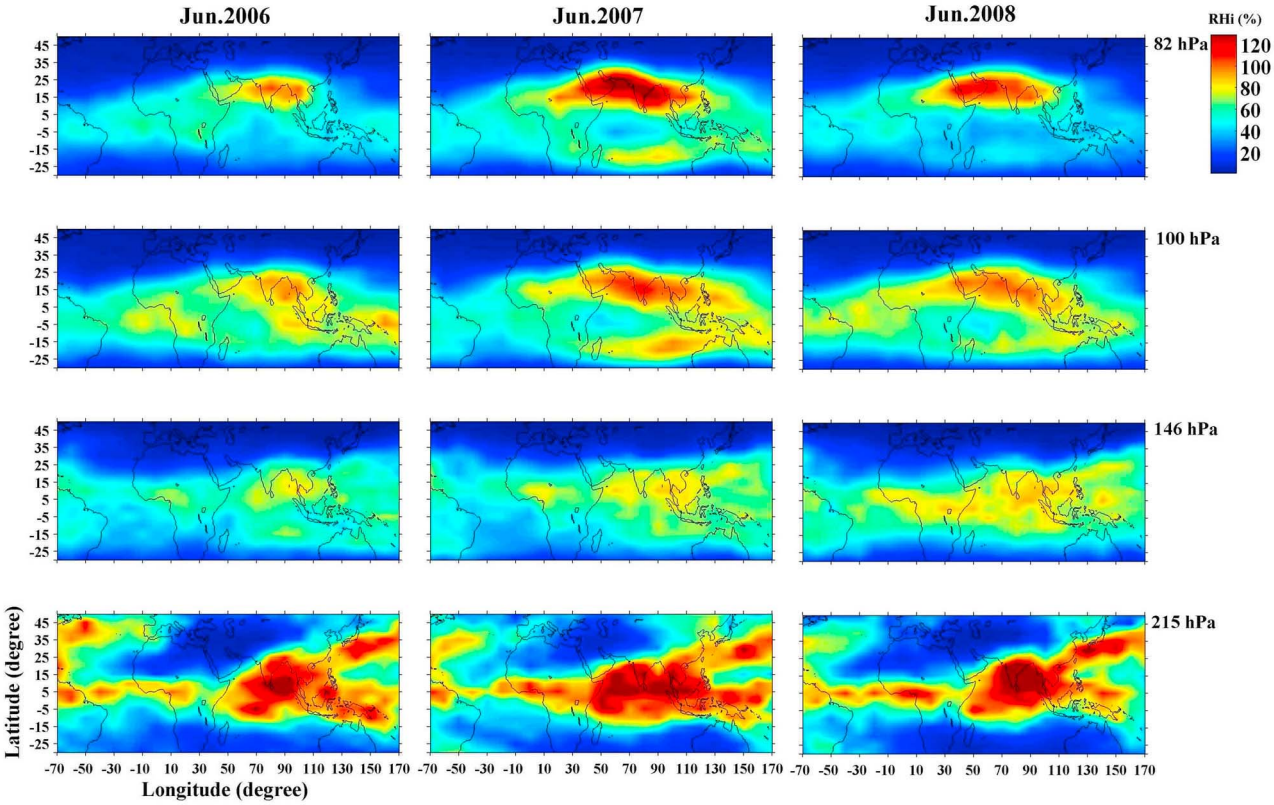

Figure 2a. Contour maps of monthly mean relative humidity with respect to ice (RHi) for different pressure levels (215, 146, 100 and 82 hPa) obtained from the AURA-MLS during June 2006 to 2008.

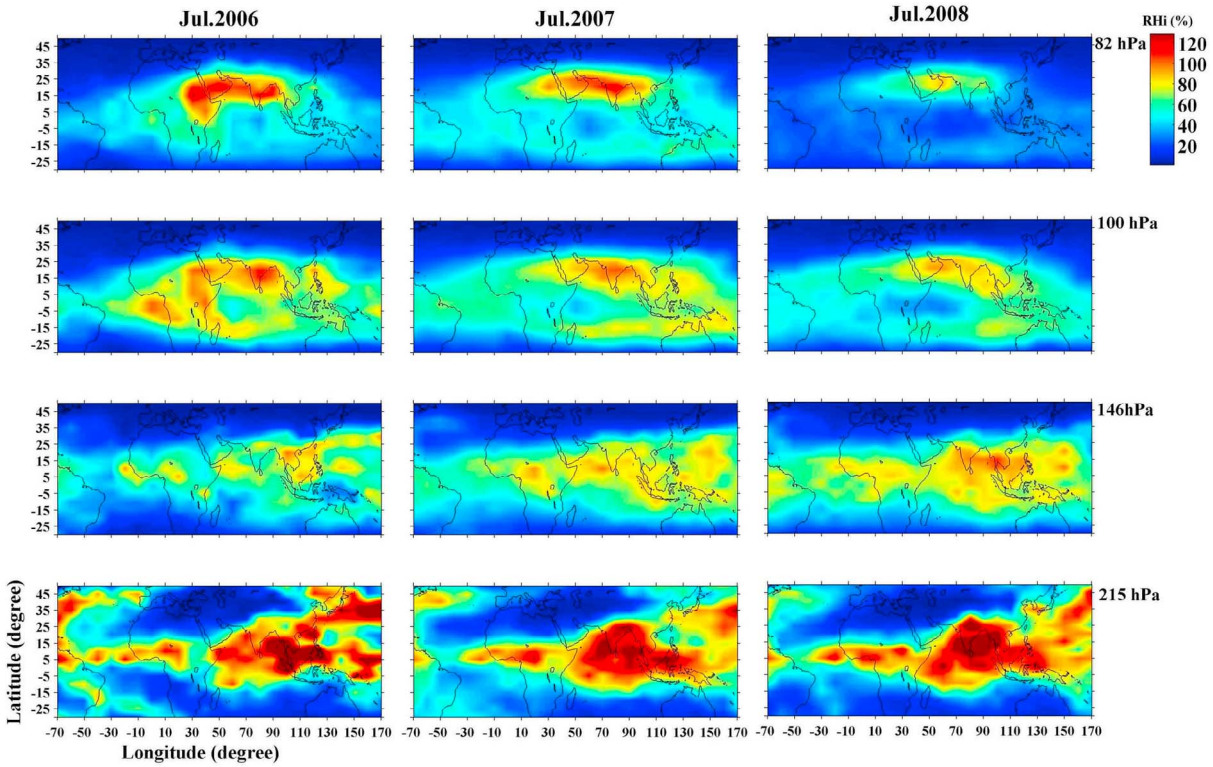

Figure 2b. Same as Figure 2a, but for July 2006 to 2008.

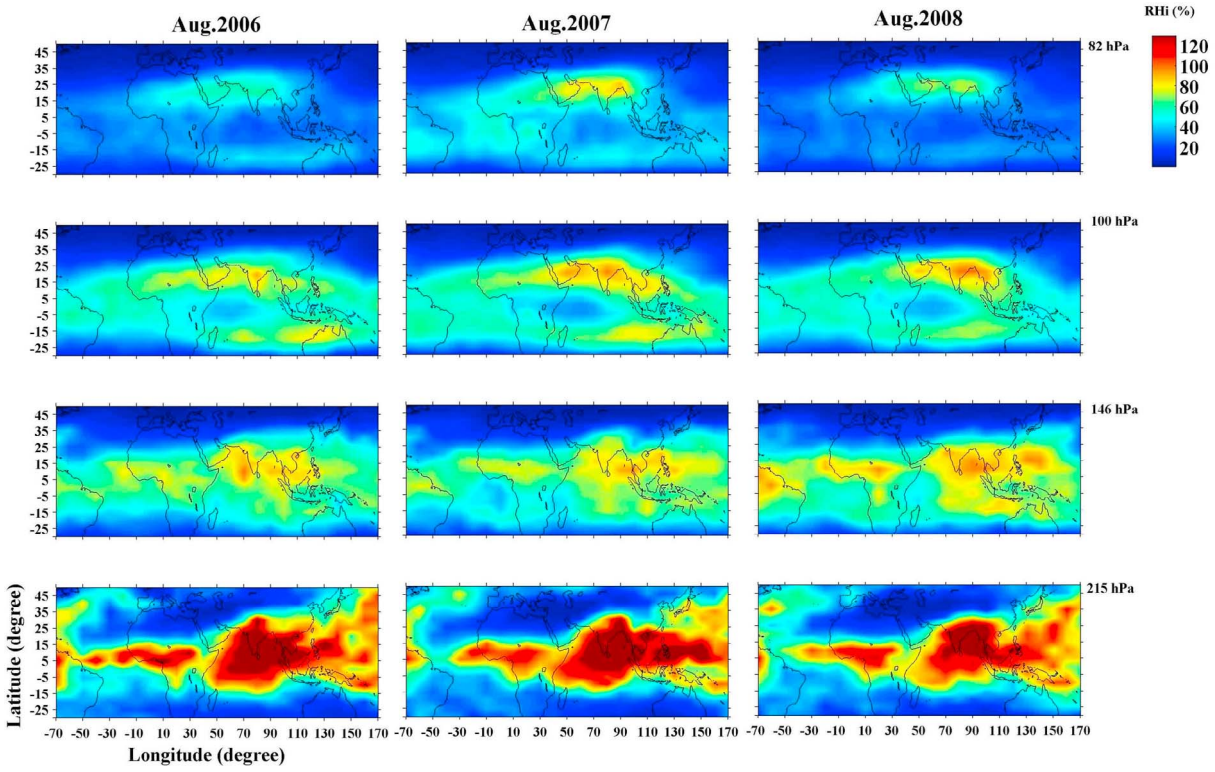

Figure 2c. Same as Figure 2a, but for August 2006 to 2008.

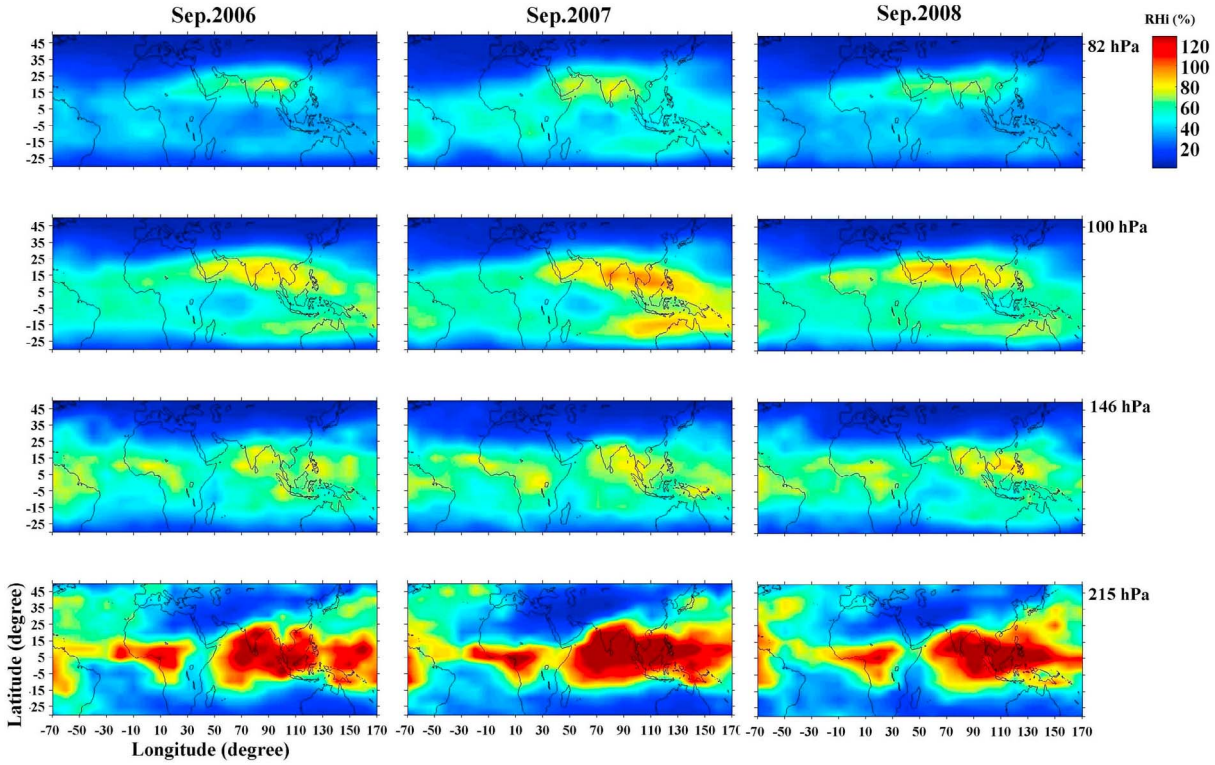

Figure 2d. Same as Figure 2a, but for September 2006 to 2008.

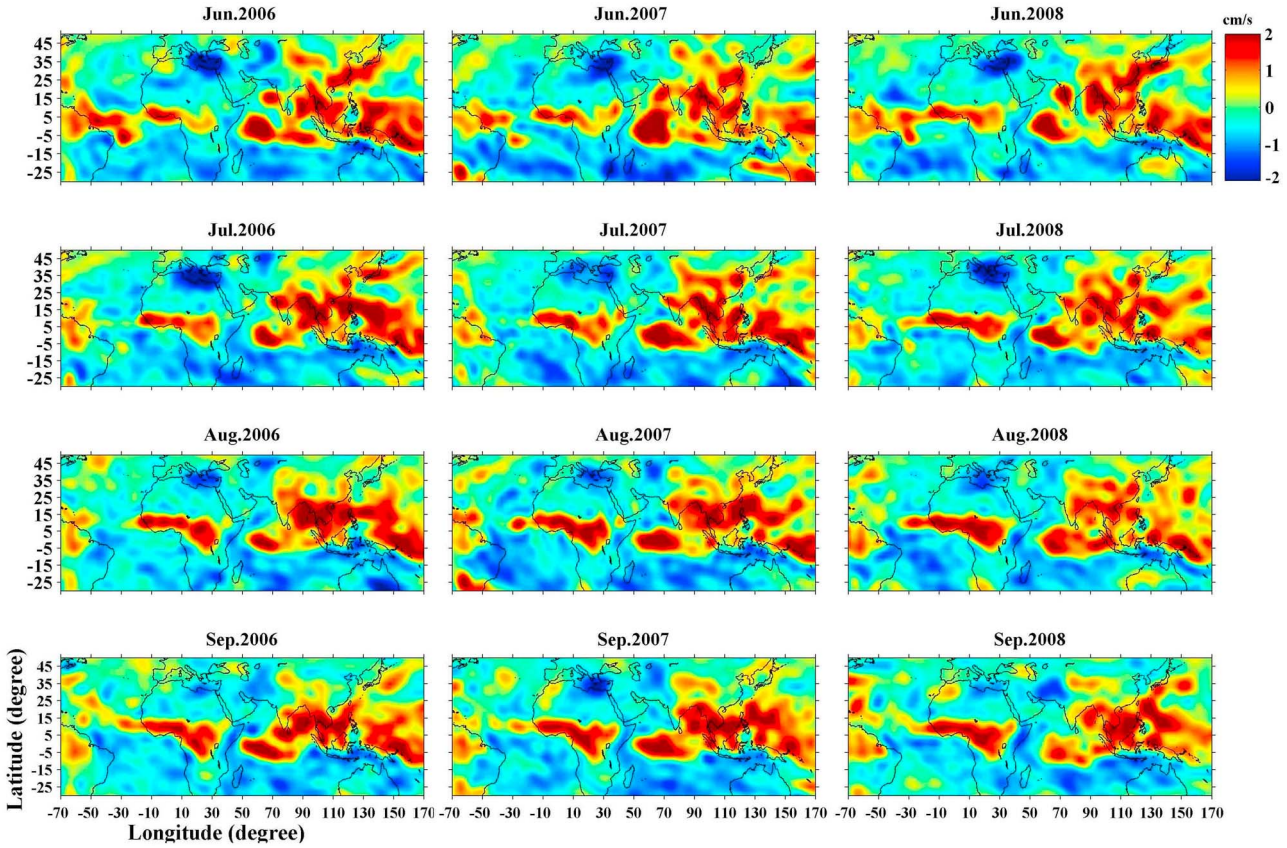

Figure 3a. Contour maps of monthly mean vertical velocity derived from the NCEP/NCAR reanalysis at the 250 hPa pressure level for June to September during 2006 to 2008.

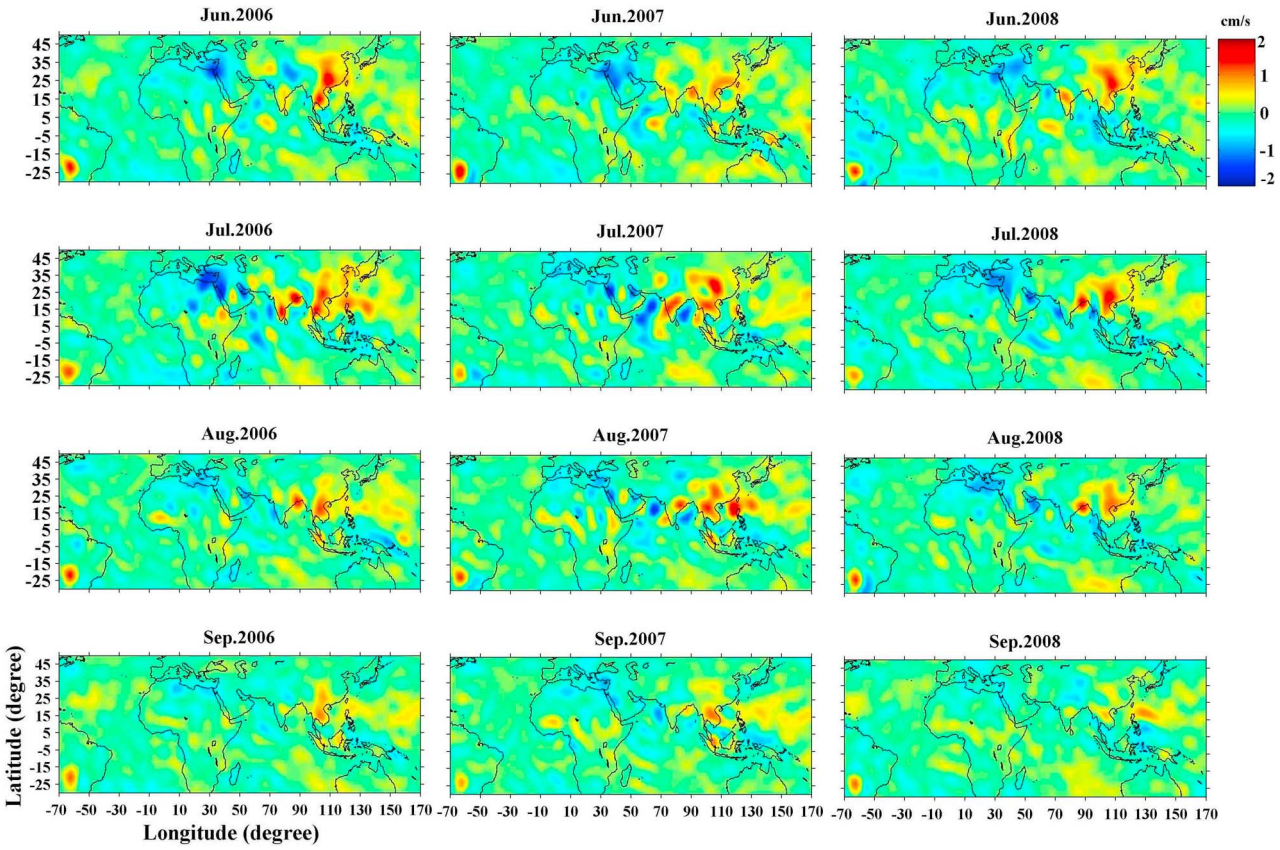

Figure 3b. Same as Figure 3a, but at the 100 hPa pressure level.

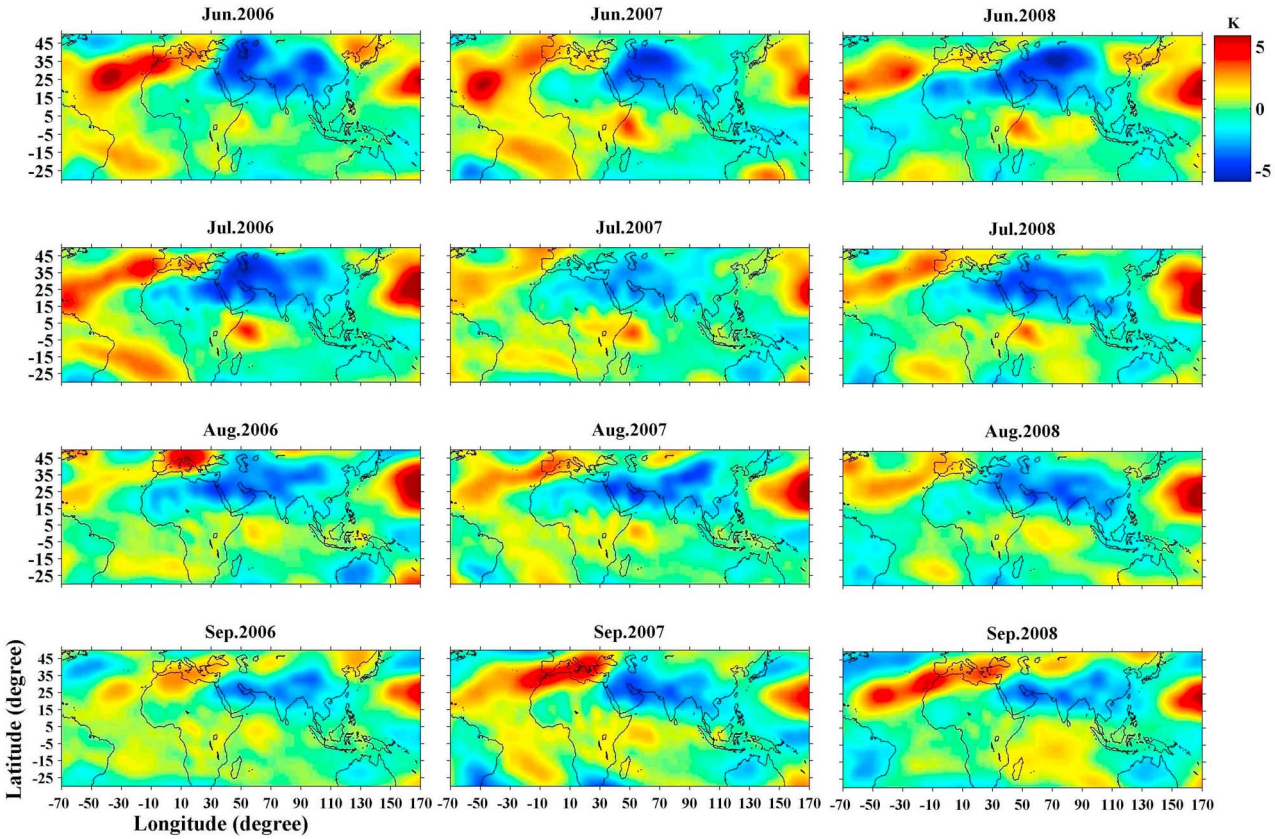

Figure 4. Contour maps of the monthly mean temperature anomalies (deviation from zonal mean) at the 100 hPa pressure level derived from the NCEP/NCAR reanalysis for June to September during 2006 to 2008.

upper troposphere and reaches up to convective outflow, from where it is transported over a larger area. During this upward displacement, air masses will cool adiabatically until the required supersaturation for the formation of ice is reached. This supports the assertion by *Luo and Rossow* [2004] that there are more cirrus clouds associated with updrafts. However, *Boehm and Verlinde* [2000] pointed out that the humidity alone is not sufficient to form cirrus clouds. Earlier studies have reported that, in addition to high humidity, cold temperature anomaly is also required for the formation of cirrus in the vicinity of the tropopause [*Immler et al.*, 2008, and references therein]. Figure 4 shows the monthly mean temperature anomaly (deviation from zonal mean) at the 100 hPa pressure level derived from the NCEP/NCAR reanalysis during June–September of 2006–2008. In the tropics, the tropopause height is usually at the 100 hPa pressure level. It is illustrated from Figure 4 that the cold tropopause temperature anomaly is observed over 15°N–40°N and 30°E–110°E, where more humidity is seen. This is one of the appropriate conditions for the formation of the tropical cirrus. However, as seen in Figure 1, the maximum cirrus is not only observed over the above favorable areas (15°N–40°N and 30°E–110°E) but also extends up to 15°S–25°N and 30°E–170°E, i.e., the ASM regions, and some parts of central west Africa. This suggests that either cirrus clouds are formed in situ due to conditions of upper tropospheric humidity that is transported from the convective zone by advection, or the clouds are formed over the convective zone and then transported, which needs to be accounted for.

[18] Figure 5 shows the contour maps of monthly mean zonal wind along with wind vectors at the 150 hPa pressure level obtained from the NCEP/NCAR reanalysis during June to September of 2006–2008. The contour maps clearly indicate the existence of the TEJ over the Indian tropical region during the ASM. By using the NCEP/NCAR reanalysis data from 1979 to 1990, *Sathiyamoorthy et al.* [2007] showed the intraseasonal variability of the TEJ over the Asian region with an intense TEJ migrating over the Indian peninsular region during the ASM. The phenomenon of seasonal reversal of winds during the ISM (June–September) due to land-sea interaction is well reported in the literature [e.g., *Hastenrath*, 1991]. This aspect can play an important role in transport of upper tropospheric humidity and the formation of tropical cirrus over those areas during the NH summer [*Hartmann*, 1994; *Ahrens*, 2003].

[19] In the month of June with the onset of the monsoon, a large amount of cirrus clouds are formed over the North Indian Ocean, Indian peninsular region, Bay of Bengal, some parts of the South China Sea, Philippine Sea, and central east Africa, as seen in Figure 1. During this month, the easterly wind prevails over these areas with magnitudes greater than -20 m s^{-1} at the 150 hPa pressure level, as shown in Figure 5. One can also note a closed circulation pattern from central Africa toward the Tibetan Plateau

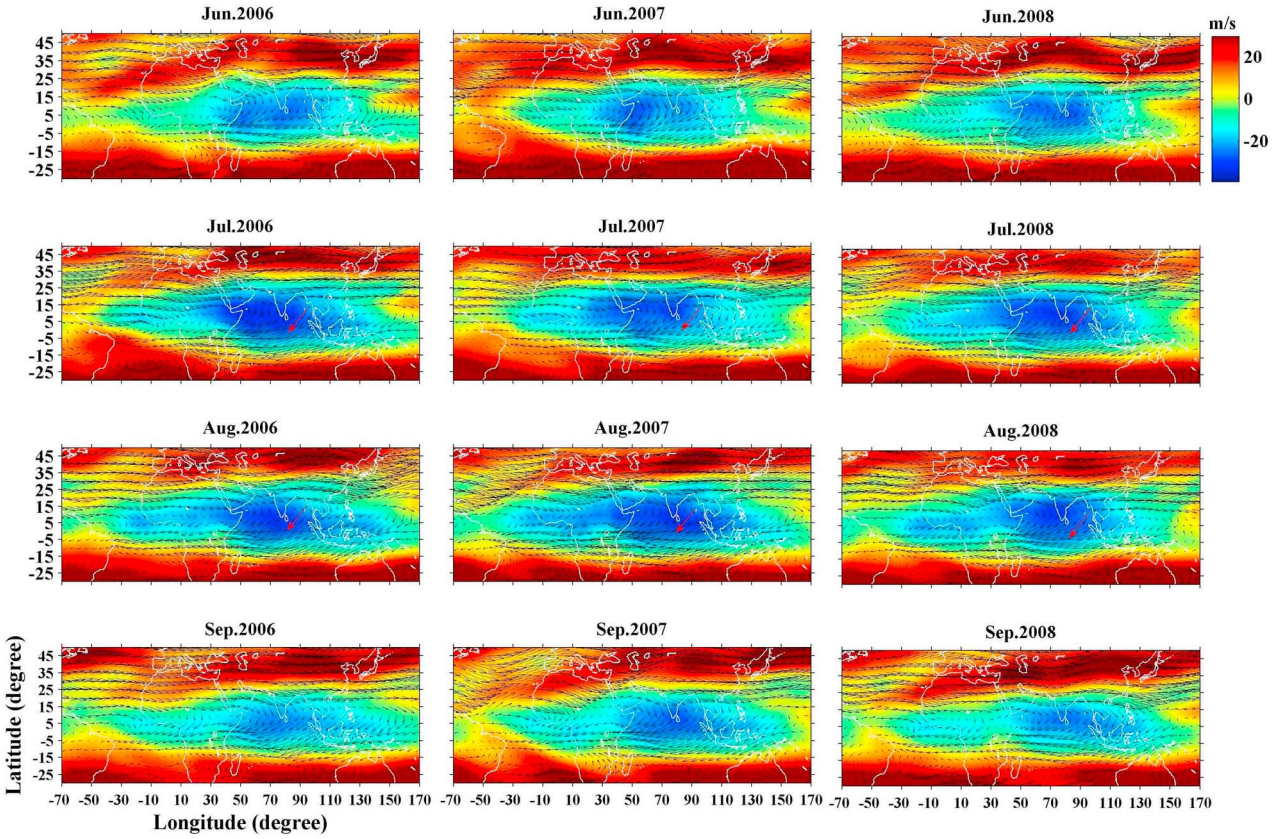

Figure 5. Contour maps of the monthly mean zonal velocity along with wind vectors derived from the NCEP/NCAR reanalysis at the 150 hPa pressure level for June to September during 2006 to 2008. Red arrow indicates the movement of Northeasterly winds.

region. *Dunkerton* [1995] reported that this circulation is associated with the ASM, which encompasses a westerly jet in the midlatitudes and an easterly jet in the tropics. From July to September, the maximum occurrence of cirrus clouds is still observed over the North Indian Ocean, Bay of Bengal, South China Sea, and Philippine Sea, but those over the Arabian Sea decrease by moving to the south. Moreover, though cirrus clouds are also observed over Central America, there is no feature of such an easterly jet in that region (not shown). Furthermore, the cirrus clouds over Central America retreat to South America by the end of October (not shown).

[20] Analysis reveals that at the 150 hPa pressure level, where the core of the TEJ is located, prominent features of cirrus clouds are observed during July to September, in particular, over Southeast Asia and the North Indian Ocean region. In October, when the TEJ moves southward and begins to decay, the occurrence of cirrus is reduced over the ASM region (not shown). This evidence clearly indicates that the TEJ is one of the driving mechanisms for the redistribution of upper tropospheric water vapor and hence the formation of the tropical cirrus over the Southeast Asian and Indian regions during the summer monsoon. *Holton and Gettelman* [2001] proposed the concept of horizontal transport of water vapor for the formation of cirrus clouds over the tropical region. In the TEJ belt, the strong advection of upper tropospheric humidity plays a major role in the formation of cirrus clouds, if the humidity is high enough. Thus, the water vapor pumped up by the convection over the North Bay of Bengal can be transported to the TEJ region by the northeasterly winds. The humidity further gets advected and redistributed over the maximum convective outflow, which is one of the mechanisms for the formation/distribution of tropical cirrus. However, at this juncture one cannot say much about the formation of cirrus in situ.

[21] Figure 6a (left) shows a contour map for the pressure level-latitude intensity (PLI) of the cirrus occurrence frequency, averaged over 30°E–120°E, from July to September of 2006, respectively. Figures 6b (left) and 6c (left) show the occurrence during June–September of 2007 and 2008, respectively. Keeping in view the TEJ band, this range of zonal mean is considered. Figures 6a, 6b, and 6c clearly show that the occurrence of cirrus is maximized between 5°S and 20°N at the height region of 200–100 hPa (12–16 km). It is also to be noted that the mean tropical tropopause height is about 100 hPa (~16 km). Thus, the occurrence of tropical cirrus is beneath the tropopause. To investigate corresponding TEJ effects, we have analyzed the corresponding zonally averaged (30°E–120°E) winds as shown in Figures 6a (right), 6b (right), and 6c (right) as height-latitude intensity maps. It can be seen that the peak intensity of zonal wind > $|-20|$ m s^{-1} occurs in the vicinity of the tropical tropopause. This shows the correlative occurrence of cirrus with the location of the easterly wind, both in height and latitude. It is worth noting that there is a consistent similarity between the latitudinal movements of the cirrus clouds and those of the easterly winds, indicating the exis-

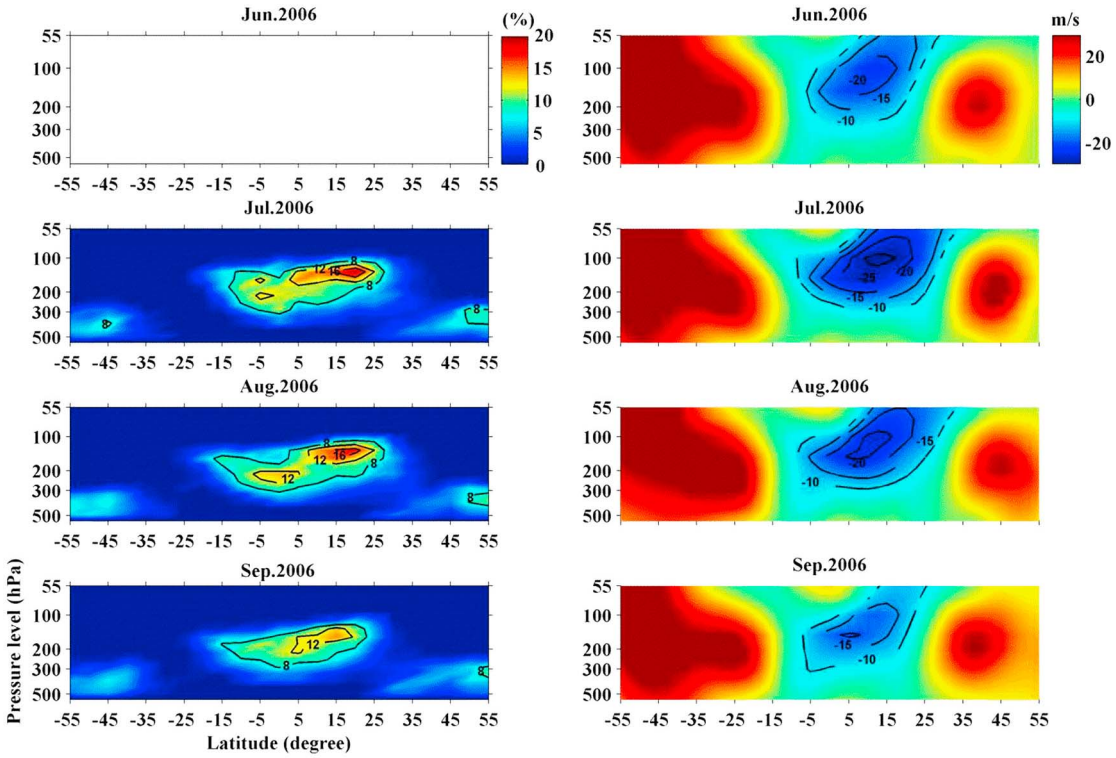

Figure 6a. Pressure level-latitude intensity maps of the percentage occurrence of (left) cirrus and (right) zonal wind averaged over 30°E–120°E for June to September in 2006, respectively. The blank areas denote no data.

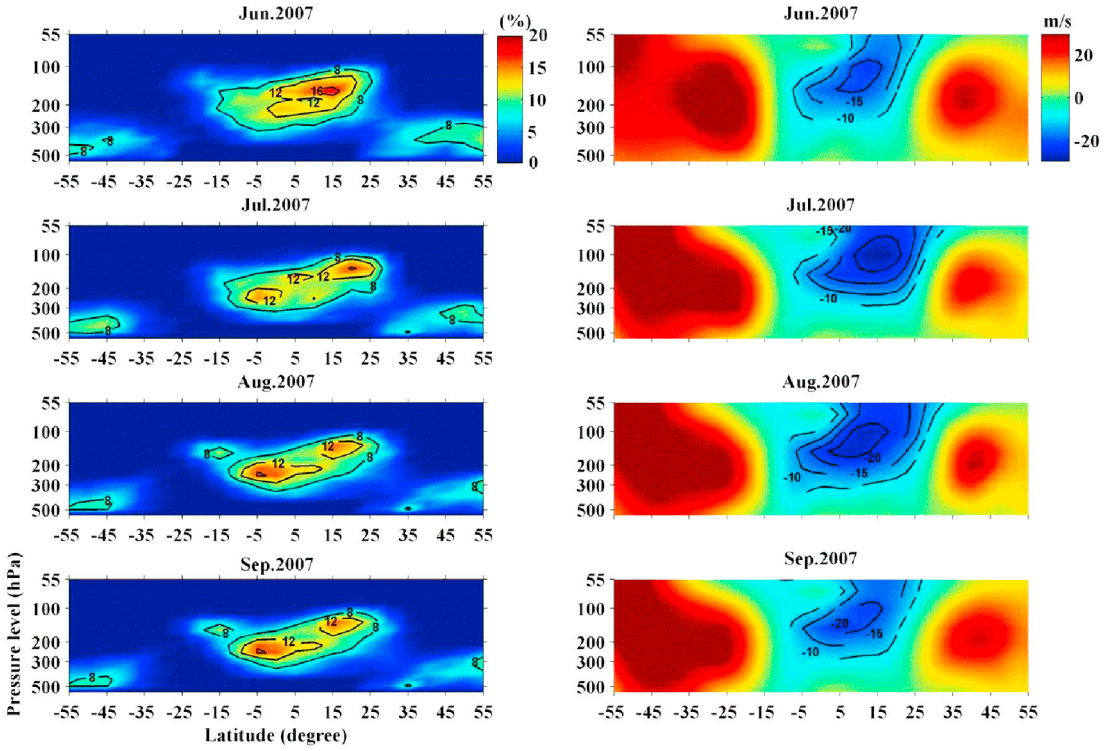

Figure 6b. Same as Figure 6a, but for 2007.

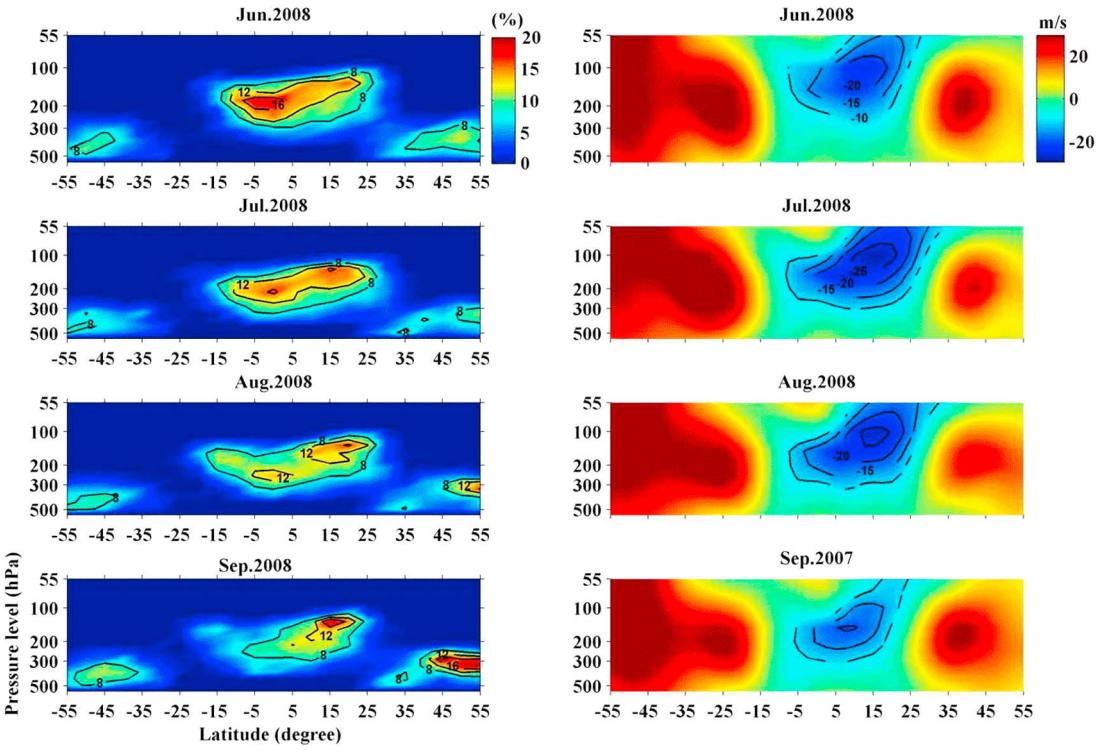

Figure 6c. Same as Figure 6a but for 2008.

tence of a strong link between them. During June to September, strong easterly winds prevail from 5°S to 20°N, while more cirrus clouds are also formed in the same latitudinal band. The generation of the tropical cirrus due to the cumulonimbus outflow from convective regions as part of the Hadley cell circulations may also cause the tropical cirrus to exist and move to longer distances from the convective area [*Wylie*, 2002].

[22] In order to elucidate the temporal and spatial evolution of the cirrus, we have constructed the month-latitude contour maps of the cirrus occurrence and zonal wind, averaged over 30°E–120°E, from 2006 to 2008 as shown in Figures 7a and 7b, respectively. Figures 7a and 7b depict the latitudinal occurrence of the cirrus in different months. Interestingly, it is observed that during June to August, the maximum occurrence of cirrus is over latitudes 5°S–15°N, which coincides with the zonal wind maxima. Once the intensity of zonal wind decreases after the summer, the occurrence of cirrus also decreases by moving to the Southern Hemisphere up to 20°S. Thus, it can be considered that the formation and dissipation of cirrus clouds over the Indian and Southeast

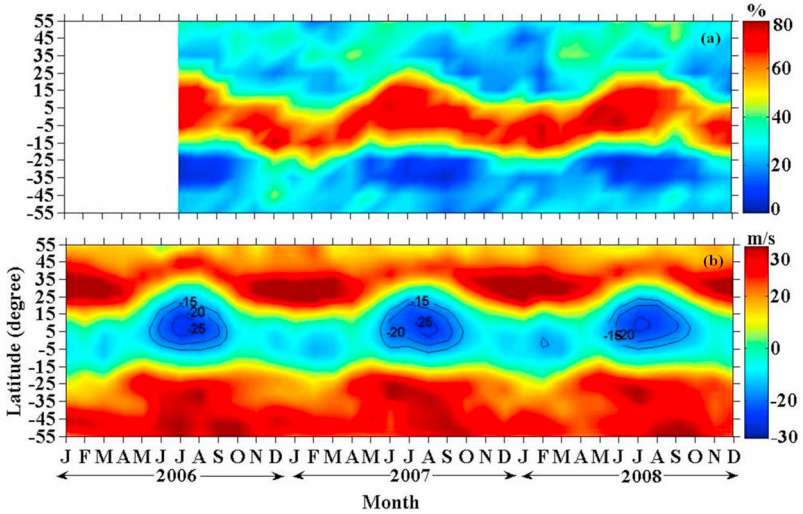

Figure 7. Month-latitude contour maps of (a) the occurrence of cirrus clouds, and (b) the zonal wind averaged over 30°E–120°E from 2006 to 2008. The blank areas denote no data.

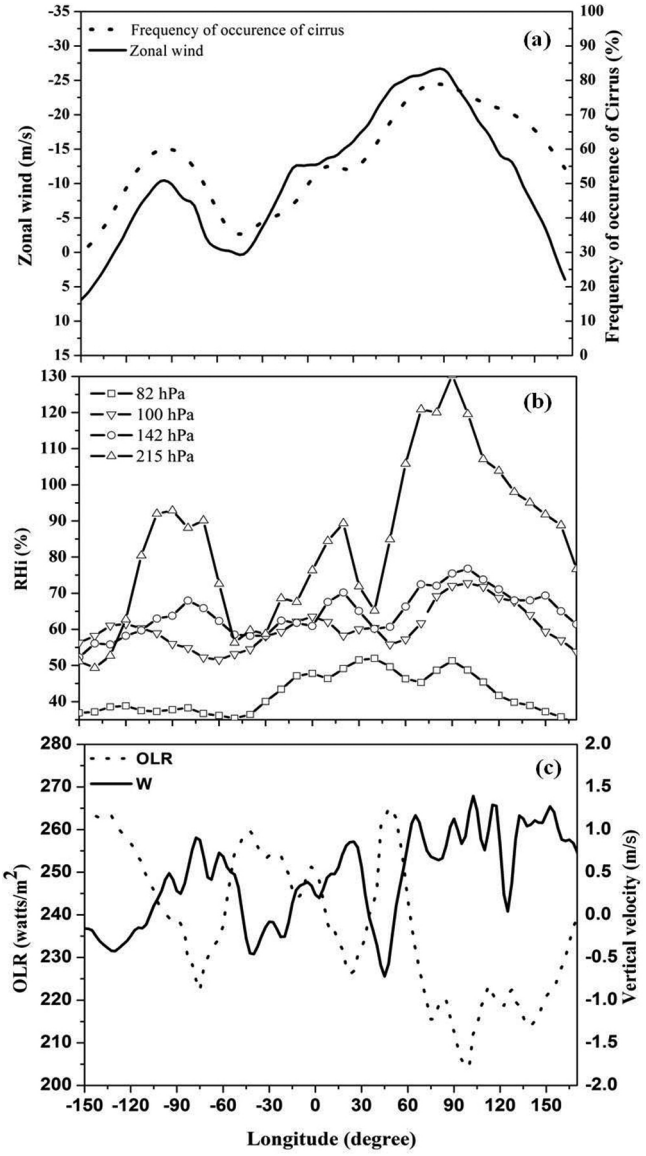

Figure 8. Longitudinal variation of (a) zonal wind and percentage of occurrence of cirrus (b) RHi at different pressure levels and (c) OLR with vertical velocity (w) at 250 hPa. Data are averaged over 5°S–15°N from June to September during 2006 to 2008.

Asian regions during the NH summer is strongly coupled with the TEJ.

[23] In order to better understand the relationship between the TEJ and cirrus cloud formation, the longitudinal variation of both the zonal wind at the 150 hPa pressure level and the occurrence of cirrus clouds, averaged from June to September for 2006–2008 (except for June 2006) with the latitudinal average over 5°S–15°N, are shown in Figure 8a. The percentage occurrence of cirrus cloud peaks over longitudes in 60°E–90°E. It is noteworthy that the easterly jets also peak in the same longitudes in the Indian and Southeast Asian regions as shown in Figure 8a. The zonal wind at the 150 hPa pressure level at these longitudes shows a close correlation between the TEJ and cirrus clouds. In the following months starting with October, the strength of the TEJ decreases and the cirrus clouds move toward the southern part of the Indian Ocean with the completion of the ASM. Thus, it can be considered that the high amount of cirrus clouds formed over the Indian and Southeast Asian region during the NH summer is due to the advection associated with the TEJ. Though the strength of the TEJ decreases at 120°E, the cirrus occurrence extends up to 170°W (not shown). This may be due to the zonal movement, i.e., Walker circulation. The nonuniform heating of land and ocean at the tropical region drives the Walker circulation, in which the air rises at the longitudes of heating (over the Indonesian region) and sinks at the longitudes of cooling (west coast of South America).

[24] Figure 8b shows the longitudinal variation of RHi at the 215, 142, 100, and 82 hPa pressure levels, averaged between June–September of 2006–2008 and over latitudes 5°S–15°N. Figure 8b clearly shows that the maximum humidity is observed over 60°E–90°E at the 215 hPa pressure level. Similarly, the longitudinal variations of OLR and the vertical velocity at 250 hPa shown in Figure 8c illustrate that less OLR (<220 W m^{-2}) with relatively strong updraft is observed over the 60°E–90°E region. All this evidence clearly indicates that the convection over the North Bay of Bengal plays a major role in transporting the humidity from the surface to the middle and the upper troposphere up to ~215 hPa, and then the TEJ facilitates the transport or redistribution of the upper tropospheric humidity over the entire Indian peninsular region.

[25] In order to conduct a quantitative statistical investigation, we have performed correlation analyses between various parameters by considering the data from 5°S to 15°N and 30°E to 150°E. Figure 9 shows the scatterplot between the cirrus occurrence frequency and OLR. Figure 9 exemplifies that even with high OLR (>220 W m^{-2}), there persists a higher percentage of cirrus occurrence. As discussed above, smaller OLR (<220 W m^{-2}) will have more deep clouds and consequently more moisture content at higher heights as one of the favorable conditions for the formation of cirrus. However, the present case is in contrast to the normal mechanism for the formation of cirrus. Figure 10 shows the scatterplot between the cirrus

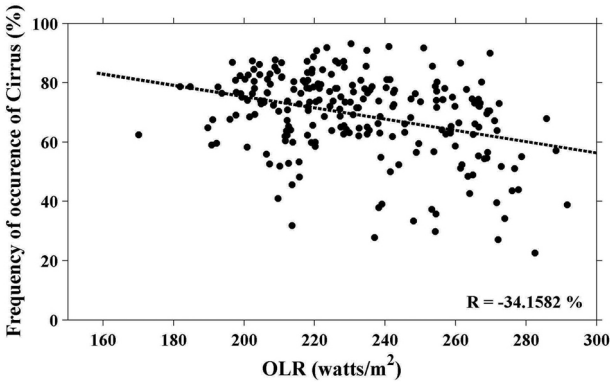

Figure 9. Scatterplot of the cirrus occurrence frequency and OLR, averaged over 5°S to 15°N and 30°E to 150°E. Dashed line gives the linear fit of the points, and R is the correlation coefficient.

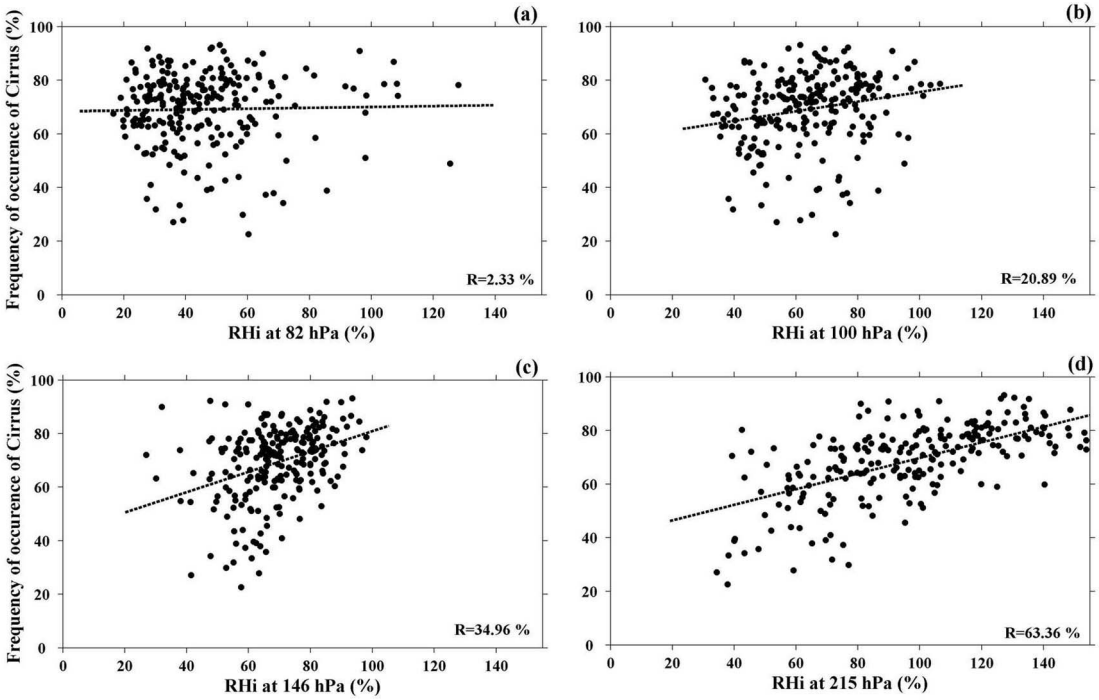

Figure 10. Scatterplots of the cirrus occurrence and RHi at pressure levels (a) 82 hPa, (b) 100 hPa, (c) 146 hPa, and (d) 215 hPa. Data are averaged over 5°S to 15°N and 30°E to 150°E. Dashed line gives the linear fit of points, and R is the correlation coefficient.

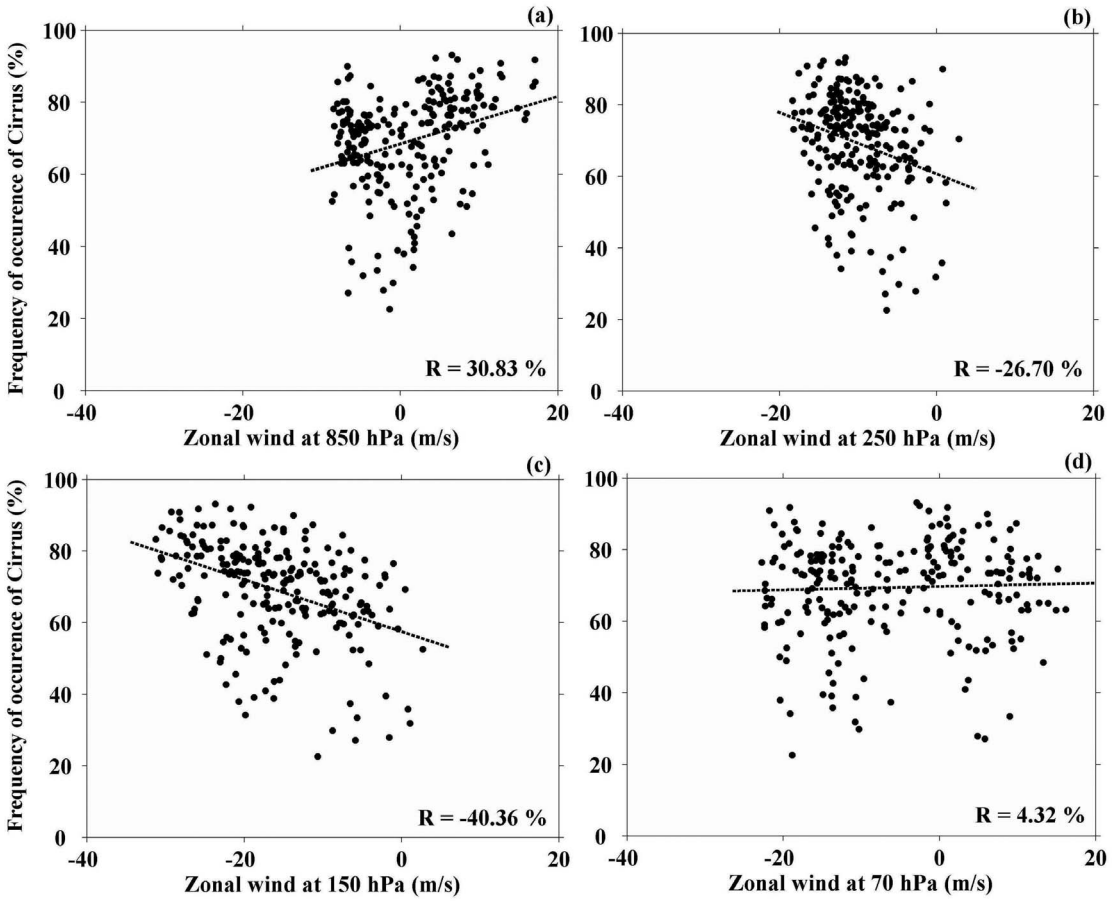

Figure 11. Scatterplots of the cirrus occurrence and zonal wind at (a) 850 hPa, (b) 250 hPa, (c) 150 hPa, and (d) 70 hPa pressure levels. Data are averaged over 5°S to 15°N and 30°E to 150°E. Dashed line gives the linear fit of the points, and R is the correlation coefficient.

occurrence and RHi at four different pressure levels. The correlations are found to be 2.3%, 20.9%, 34.9%, and 63.4% at 82, 100, 146, and 215 hPa, respectively. Thus, it is clear that humidity at the 215 hPa pressure level plays a major role in the formation of cirrus. Figure 11 shows the scatterplots for the cirrus occurrence versus zonal wind at four different pressure levels. The correlations are about 30.8%, −26.7%, −40.4%, and 4.3% at 850, 250, 150, and 70 hPa, respectively. This shows that the easterly zonal wind at the 150 hPa pressure level, where the maximum TEJ strength is observed as discussed earlier, contributes more to the formation and distribution of the tropical cirrus. The coefficient of multiregression analysis between cirrus occurrence frequency with the zonal wind at 150 hPa, RHi at 215 hPa, and OLR is found to be 64.8%. By doing a two-dimensional cross-correlation analysis, we studied the spatial correlation statistics to assess how well the cirrus occurrence is correlated with the zonal wind maxima. We have considered the data from 25°S to 45°N, and 70°W to 170°E. Both the cirrus occurrence frequency and zonal wind are averaged between June–September of 2006–2008 (except for the cirrus occurrence frequency of June 2006). Figure 12 shows the results of this investigation, where lags of both values are zeros indicating that the maximum cirrus occurrence is well correlated with zonal wind maxima in the spatial domain.

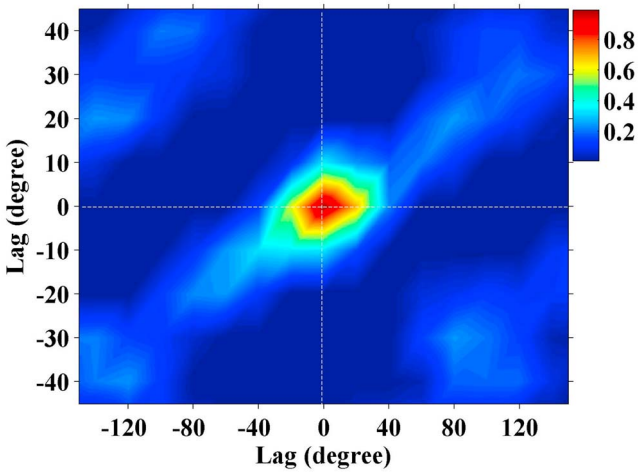

Figure 12. The two-dimensional cross-correlation analysis between cirrus occurrence frequency and the magnitude of zonal wind. The correlation coefficients are normalized as shown in the color bar.

[26] *Menzel et al.* [1992] have studied the relationship between the jet streams at 300 hPa and cirrus clouds for four years over the geographical area 27°N to 51°N and 60°W to 140°W by using data of the geostationary Visible-Infrared Spin Scan Radiometer Atmospheric Sounder (VAS). They reported that the occurrence of cirrus clouds is about 40–60% in the months of the strong jet stream (>35 m s^{-1}) and is reduced to 10–30% in the weak stream months. *Haynes and Stephens* [2002] showed that the highest frequency of occurrence of cirrus clouds is found in the specific (accelerating) regions of the jet stream. Our analysis also shows the occurrence of cirrus is about 70–80% during the months of the strong jet stream and decreases to nearly 30–40% in the non–jet stream periods, averaged over the study areas. *Menzel et al.* [1992] have shown that there is no significant change in the frequency of occurrence of cirrus clouds with wind speeds. In contrast to this finding, the present analysis shows that the occurrence of cirrus increases with the strength of the jet stream as revealed from Figure 11c. However, we cannot exclude other factors apart from the TEJ that may also affect the transport and redistribution of upper tropospheric humidity resulting in the formation of the tropical cirrus. These issues will be considered for our near future goal.

4. Summary and Concluding Remarks

[27] The redistribution and transport of the upper tropospheric humidity and then the formation mechanism of the tropical cirrus clouds coupled with the tropical easterly jet are investigated by using combined data of CALIPSO, Aura-MLS, and NCEP/NCAR reanalysis from 2006 to 2008. The following features are brought out from the present observations:

[28] 1. A low value of OLR (<220 W m^{-2}) is seen over the North Bay of Bengal during the South Asian summer monsoon with a high occurrence of cirrus observed based on CALIPSO data.

[29] 2. During the same months, more humidity is observed in the upper troposphere over the tropical Arabian Sea, Indian Ocean, Indian peninsular region, Bay of Bengal, South China Sea, and Philippine Sea, and a higher percentage of cirrus formed over the same regions.

[30] 3. There is a transport of humidity from the lower to the upper troposphere, as revealed from the vertical velocity, above the convective areas (e.g., low values of OLR over the North Bay of Bengal), and then it is further advected and redistributed over the maximum convective outflow caused by the elongated easterly tropical jet, or TEJ.

[31] 4. We conclude from a few correlated studies that the observed high frequency of occurrence of cirrus over the South Asian summer monsoon region is closely associated with the redistribution of upper tropospheric water vapor advected by the TEJ.

[32] 5. Thus, the present study for the first time brings out the crucial role of the TEJ in the distribution of the upper tropospheric humidity and subsequent formation of cirrus clouds during the Asian summer monsoon.

[33] **Acknowledgments.** We appreciate receiving the data from various sources including the CALIPSO data from the NASA Langley Research Center Atmospheric Science Data Center, MLS data from the Goddard Earth Sciences Data and Information Services Centre, and the NCEP/NCAR reanalysis data from the NOAA-CIRES Climate Diagnostics Centre (http://www.cdc.noaa.gov). S. K. Das was supported by the Taiwan scholarship during this study and would like to acknowledge the Taiwan Government and the National Central University, Chung-Li. Authors gratefully acknowledge all the reviewers for their constructive comments and suggestions for the improvement of the manuscript. This work is supported by the National Science Council of Republic of China (ROC) through a grant NSC99-2010-2111-M08-307.

References

Ahrens, C. D. (2003), *Meteorology Today: An Introduction to Weather, Climate, and the Environment*, Thompson Brooks Cole, Pacific Grove, Calif.

Basist, A. N., and M. Chelliah (1997), Comparison of tropospheric temperature derived from the NCEP/NCAR reanalysis, NCEP operational analysis, and the microwave sounding unit, *Bull. Am. Meteorol. Soc.*, *78*, 1431–1447, doi:10.1175/1520-0477(1997)078<1431:COTTDF>2.0.CO;2.

Boehm, M. T., and J. Verlinde (2000), Stratospheric influence on upper tropospheric tropical cirrus, *Geophys. Res. Lett.*, *27*, 3209–3212, doi:10.1029/2000GL011678.

Clark, H. L. (2005), Longitudinal variability of water vapor and cirrus in the tropical tropopause layer, *J. Geophys. Res.*, *110*, D07107, doi:10.1029/2004JD004943.

Corti, T., B. P. Luo, T. Peter, H. Voemel, and Q. Fu (2005), Mean radiative energy balance and vertical mass fluxes in the equatorial upper troposphere and lower stratosphere, *Geophys. Res. Lett.*, *32*, L06802, doi:10.1029/2004GL021889.

De Mott, P. (2002), Laboratory studies of cirrus cloud processes, in *Cirrus*, edited by D. Lynch et al., pp. 102–135, Oxford Univ. Press, New York.

Dowling, D. R., and L. F. Radke (1990), A summary of the physical properties of cirrus clouds, *J. Appl. Meteorol.*, *29*, 970–978, doi:10.1175/1520-0450(1990)029<0970:ASOTPP>2.0.CO;2.

Dunkerton, T. J. (1995), Evidence of meridional motion in the summer lower stratosphere adjacent to monsoon regions, *J. Geophys. Res.*, *100*, 16,675–16,688, doi:10.1029/95JD01263.

Francis, P. N., J. S. Foot, and A. J. Baran (1999), Aircraft measurements of the solar and infrared radiative properties of cirrus and their dependence on ice crystal shape, *J. Geophys. Res.*, *104*, 31,685–31,695, doi:10.1029/1999JD900438.

Gettelman, A., W. J. Randel, F. Wu, and S. T. Massie (2002), Transport of water vapor in the tropical tropopause layer, *Geophys. Res. Lett.*, *29*(1), 1009, doi:10.1029/2001GL013818.

Hartmann, D. L. (1994), *Global Physical Climatalogy*, Academic, San Diego, Calif.

Hartmann, D. L., J. R. Holton, and Q. Fu (2001), The heat balance of the tropical tropopause, cirrus, and stratospheric dehydration, *Geophys. Res. Lett.*, *28*, 1969–1972, doi:10.1029/2000GL012833.

Hastenrath, S. (1991), Regional circulation systems, in *Climate Dynamics of the Tropics*, pp. 114–218, Kluwer Acad., Dordrecht, Netherlands.

Haynes, J. M., and G. L. Stephens (2002), A composite and microphysical study of jet stream cirrus over the ARM site, paper presented at Twelfth ARM Science Team Meeting, Atmos. Radiat. Meas. Program, St. Petersburg, Fla.

Heymsfield, A. J., and G. M. McFarquhar (2002), Mid-latitude and tropical cirrus: Microphysical properties, in *Cirrus*, edited by D. Lynch et al., pp. 78–101, Oxford Univ. Press, New York.

Holton, J. R., and A. Gettelman (2001), Horizontal transport and the dehydration of the stratosphere, *Geophys. Res. Lett.*, *28*, 2799–2802, doi:10.1029/2001GL013148.

Immler, F., K. Krüger, M. Fujiwara, G. Verver, M. Rex, and O. Schrems (2008), Correlation between equatorial Kelvin waves and the occurrence of extremely thin ice clouds at the tropical tropopause, *Atmos. Chem. Phys.*, *8*, 4019–4026, doi:10.5194/acp-8-4019-2008.

James, R., M. Bonazzola, B. Legras, K. Surbled, and S. Fueglistaler (2008), Water vapor transport and dehydration above convective outflow during Asian monsoon, *Geophys. Res. Lett.*, *35*, L20810, doi:10.1029/2008GL035441.

Jensen, E. J., O. B. Toon, H. B. Selkirk, J. D. Spinhirne, and M. A. Schoeberl (1996), On the formation and persistence of subvisible cirrus clouds near the tropical tropopause, *J. Geophys. Res.*, *101*, 21,361–21,375, doi:10.1029/95JD03575.

Kalnay, E., et al. (1996), The NCEP/NCAR 40-year reanalysis project, *Bull. Am. Meteorol. Soc.*, *77*, 437–471, doi:10.1175/1520-0477(1996)077<0437:TNYRP>2.0.CO;2.

Khvorostyanov, V. I., and K. Sassen (2002), Microphysical processes in cirrus and their impact on radiation: A mesoscale modeling perspective,

in *Cirrus*, edited by D. Lynch et al., pp. 397–432, Oxford Univ. Press, New York.

Kim, S. W., S. Berthier, J. C. Raut, P. Chazette, F. Dulac, and S. C. Yoon (2008), Validation of aerosol and cloud layer structures from the space-borne lidar CALIOP using a ground-based lidar in Seoul, Korea, *Atmos. Chem. Phys.*, *8*, 3705–3720, doi:10.5194/acp-8-3705-2008.

Koteswaram, P. (1958), The easterly jet stream in the tropics, *Tellus*, *10*, 43–57, doi:10.1111/j.2153-3490.1958.tb01984.x.

Lamquin, N., C. J. Stubenrauch, and J. Pelon (2008), Upper tropospheric humidity and cirrus geometrical and optical thickness: Relationships inferred from one year of collocated AIRS-CALIPSO data, *J. Geophys. Res.*, *113*, D00A08, doi:10.1029/2008JD010012.

Liebmann, B., and C. A. Smith (1996), Description of a complete (interpolated) outgoing longwave dataset, *Bull. Am. Meteorol. Soc.*, *77*, 1275–1277.

Liou, K. N. (1986), Influence of cirrus clouds on weather and climate processes: A global perspective, *Mon. Weather Rev.*, *114*, 1167–1199, doi:10.1175/1520-0493(1986)114<1167:IOCCOW>2.0.CO;2.

Livesey, N. J., et al. (2007), Earth Observing Systems (EOS) Microwave Limb Sounder (MLS) Version 2.2 level 2 data quality and description document, version 2.2 _ _1.0a, report, Jet Propul. Lab., Pasadena, Calif.

Luo, Z., and W. B. Rossow (2004), Characterizing tropical cirrus life cycle, evolution and interaction with upper tropospheric water vapor using Lagrangian trajectory analysis of satellite observations, *J. Clim.*, *17*, 4541–4563, doi:10.1175/3222.1.

Mace, G. G., M. Deng, B. Soden, and E. Zipser (2006), Association of tropical cirrus in the 10–15-km layer with deep convective sources: An observational study combining millimeter radar data and satellite-derived trajectories, *J. Atmos. Sci.*, *63*, 480–503, doi:10.1175/JAS3627.1.

Menzel, W. P., D. P. Wylie, and K. I. Strabala (1992), Seasonal and diurnal changes in cirrus clouds as seen in four years of observations with the VAS, *J. Appl. Meteorol.*, *31*, 370–385, doi:10.1175/1520-0450(1992)031<0370:SADCIC>2.0.CO;2.

Nazaryan, H., M. P. McCormick, and W. P. Menzel (2008), Global characterization of cirrus clouds using CALIPSO data, *J. Geophys. Res.*, *113*, D16211, doi:10.1029/2007JD009481.

Park, M., W. J. Randel, A. Gettelman, S. T. Massie, and J. H. Jiang (2007), Transport above the Asian summer monsoon anticyclone inferred from Aura Microwave Limb Sounder tracers, *J. Geophys. Res.*, *112*, D16309, doi:10.1029/2006JD008294.

Penner, J. E., D. H. Lister, D. J. Griggs, D. J. Dokken, and M. McFarland (1999), Aviation and the global atmopshere: Special report of the Intergovernmental Panel on Climate Change, Cambridge Univ. Press, Cambridge, U. K.

Platt, C. M. R. (1973), Lidar and radiometric observations of cirrus clouds, *J. Atmos. Sci.*, *30*, 1191–1204, doi:10.1175/1520-0469(1973)030<1191:LAROOC>2.0.CO;2.

Ricaud, P., B. Barret, J.-L. Attié, E. Motte, E. Le Flochmoën, H. Teyssèdre, V.-H. Peuch, N. Livesey, A. Lambert, and J.-P. Pommereau (2007), Impact of land convection on troposphere-stratosphere exchange in the tropics, *Atmos. Chem. Phys.*, *7*(21), 5639–5657, doi:10.5194/acp-7-5639-2007.

Sassen, K. (1991), The polarization lidar technique for cloud research: A review and current assessment, *Bull. Am. Meteorol. Soc.*, *72*, 1848–1866, doi:10.1175/1520-0477(1991)072<1848:TPLTFC>2.0.CO;2.

Sassen, K., and G. G. Mace (2002), Ground-based remote sensing of cirrus cloud, in *Cirrus*, edited by D. Lynch et al., pp. 168–196, Oxford Univ. Press, New York.

Sassen, K., Z. Wang, and D. Liu (2008), Global distribution of cirrus clouds from CloudSat/Cloud-Aerosol lidar and infrared pathfinder satellite observations (CALIPSO) measurements, *J. Geophys. Res.*, *113*, D00A12, doi:10.1029/2008JD009972.

Sassen, K., Z. Wang, and D. Liu (2009), Cirrus clouds and deep convection in the tropics: Insights from CALIPSO and CloudSat, *J. Geophys. Res.*, *114*, D00H06, doi:10.1029/2009JD011916.

Sathiyamoorthy, V., P. K. Pal, and P. C. Joshi (2004), Influence of the upper-tropospheric wind shear upon cloud radiative forcing in the Asian monsoon region, *J. Clim.*, *17*, 2725–2735, doi:10.1175/1520-0442(2004)017<2725:IOTUWS>2.0.CO;2.

Sathiyamoorthy, V., P. K. Pal, and P. C. Joshi (2007), Intraseasonal variability of the tropical easterly jet, *Meteorol. Atmos. Phys.*, *96*, 305–316, doi:10.1007/s00703-006-0214-7.

Savtchenko, A., R. Kummerer, P. Smith, S. Kempler, and G. Leptoukh (2008), A-train data depot-bringing atmospheric measurements together, *IEEE Trans. Geosci. Remote Sens.*, *46*, 2788–2795, doi:10.1109/TGRS.2008.917600.

Schumann, U. (2002), Contrail cirrus, in *Cirrus*, edited by D. Lynch et al., pp. 231–255, Oxford Univ. Press, New York.

Sherwood, S. C., and A. E. Dessler (2003), Convective mixing near the tropopause: Insights from seasonal variations, *J. Atmos. Sci.*, *60*(21), 2674–2685, doi:10.1175/1520-0469(2003)060<2674:CMNTTT>2.0.CO;2.

Tao, Z., M. P. McCormick, and D. Wu (2008), A comparison method for spaceborne and ground-based lidar and its application to the CALIPSO lidar, *Appl. Phys. B*, *91*, 639–644, doi:10.1007/s00340-008-3043-1.

Twomey, S. (1991), Aerosols, clouds and radiation, *Atmos. Environ.*, *25*, 2435–2442, doi:10.1016/0960-1686(91)90159-5.

Wang, P. H., P. Minnis, M. P. McCormick, G. S. Kent, and K. M. Skeens (1996), A 6-year climatology of cloud occurrence frequency from Stratospheric Aerosol and Gas Experiment II observations (1985–1990), *J. Geophys. Res.*, *101*, 29,407–29,429, doi:10.1029/96JD01780.

Waters, J. W., et al. (2006), The Earth Observing System Microwave Limb Sounder (EOS MLS) on the Aura satellite, *IEEE Trans. Geosci. Remote Sens.*, *44*(5), 1075–1092, doi:10.1109/TGRS.2006.873771.

Wild, M., and E. Roeckner (2006), Radiative fluxes in the ECHAM5 general circulation model, *J. Clim.*, *19*, 3792–3809, doi:10.1175/JCLI3823.1.

Winker, D. M., J. Pelon, and M. P. McCormick (2003), The CALIPSO mission: Space borne lidar for observation of aerosols and clouds, *Proc. SPIE*, *4893*, 1–11, doi:10.1117/12.466539.

Wu, D. L., J. H. Jiang, W. G. Read, R. T. Austin, C. P. Davis, A. Lambert, G. L. Stephens, D. G. Vane, and J. W. Waters (2008), Validation of the Aura MLS cloud ice water content measurements, *J. Geophys. Res.*, *113*, D15S10, doi:10.1029/2007JD008931.

Wylie, D. (2002), Cirrus and weather: A satellite perspective, in *Cirrus*, edited by D. Lynch et al., pp. 136–146, Oxford Univ. Press, New York.

Wylie, D. P., W. P. Menzel, H. M. Woolf, and K. I. Strabala (1994), Four years of global cirrus cloud statistics using HIRS, *J. Clim.*, *7*, 1972–1986, doi:10.1175/1520-0442(1994)007<1972:FYOGCC>2.0.CO;2.

Yang, Q., Q. Fu, and Y. Hu (2010), Radiative impacts of clouds in the tropical tropopause layer, *J. Geophys. Res.*, *115*, D00H12, doi:10.1029/2009JD012393.

C.-W. Chiang and J.-B. Nee, National Central University, Department of Physics, 300 Jhongda Rd., Chung-Li, 32001, Taiwan. (jbnee@phy.ncu.edu.tw)

S. K. Das, Indian Institute of Tropical Meteorology, PM&A Division, Pune, India.